This document is the accepted manuscript version of the following article:
Priebe, A., Dousse, B., Tzou, C. Y., Papadopoulos, G., Utke, I., Bensaoula, A., … Guerra-Nuñez, C. (2022). Real-time in situ parallel detection of elements and molecules with TOFMS during ALD for chemical quality control of thin films. Journal of Physical Chemistry C. https://doi.org/10.1021/acs.jpcc.1c09544

Real-Time In Situ Parallel Detection Of Elements And Molecules With TOFMS During ALD For Chemical Quality Control Of Thin Films

Agnieszka Priebe[1,], Bryan Dousse[1,2], Chia-Yu Tzou[3], Georgios Papadopoulos[3], Ivo Utke[1], Abdelhak Bensaoula[3], Johann Michler[1] and Carlos Guerra-Nuñez[2]*

[1]Empa, Swiss Federal Laboratories for Materials Science and Technology, Laboratory for Mechanics of Materials and Nanostructures, Feuerwerkerstrasse 39, CH-3602 Thun, Switzerland

[2]Swiss Cluster AG, Feuerwerkerstrasse 39, CH-3602 Thun, Switzerland

[3]TOFWERK AG, Schorenstrasse 39, 3645 Thun

[*]Corresponding author: agnieszka.priebe@empa.ch

Keywords: mass spectrometry, atomic layer deposition, gas precursors, thin films, fabrication, process chemistry, process analysis, process monitoring

ABSTRACT

The extraordinary properties of thin films result from their 2D structure, i.e. one dimension is negligibly small when compared with the two others. Consequently, precise and well-established fabrication methods are required to provide appropriate functionality of these materials, such as hardness, resistance to mechanical stress, durability or chemical/electrical stability. In this work, we present the potential of integrating a time-of-flight mass spectrometer (TOFMS) with atomic layer deposition (ALD) for real-time control of thin film fabrication processes. This technique provides parallel detection of all ionized molecules and ionized fragments, and therefore the limitations of commonly used quadrupole mass spectrometers are overcome. Furthermore, since the chemical data acquisition is conducted *in situ*, the results of applied deposition parameters can be observed online allowing for immediate modifications as, for example, in the case of process deviation from optimal or failure. The presented monitoring method is expected to be broadly applied in many deposition or etching processes, in which accurate chemical composition and strict endpoint control are demanded, such as manufacture of microdevices (for new energy solutions and microelectronics), protective surface coatings, actuators, sensors and for biomedical applications.

INTRODUCTION

Atomic Layer Deposition (ALD) is a type of Chemical Vapour Deposition (CVD), employing self-limiting surface reactions of typically two gaseous reactants in sequential mode.[1–3] Therefore, it ensures precise control of the film thickness whether as a single layer or a multilayer stack on planar as well as on porous substrates. Typical film thicknesses vary from several angstroms to over 100 nm.[4] Moreover, it provides extreme surface conformality, uniformity

and a lack of pinholes. Pure metals, oxides, nitrides, fluorides, sulphides, II–VI and III–V compounds can be grown with ALD.[2,5–10] Therefore, this technique is broadly used in both, industry and research centres. ALD-fabricated thin films are applied in microelectronics (for high-k dielectrics[11], micro- and nanoelectromechanical systems, MEMS[12,13] and NEMS[14]), photovoltaics[4], in fabrication of $Cu(In,Ga)Se_2$ thin film solar cells[15–18], dye-sensitized solar cells (DSSCs)[4,19], organic photovoltaics[4,20], organic light-emitting diodes (OLED)[21–23], transparent conducting oxides[4] (TCOs, such as SnO_2[3,24], ZnO[25], Al:ZnO[26], black silicon[27]), anti-reflective coatings[4,12], coatings protecting against corrosion[28,29], thin film electroluminescent (TFEL) displays[2], in semiconductor and energy conversion devices[5,30], in medical applications[31], for battery cycle life time improvement, as well as for fabricating dedicated model samples used for developing and validating the potential of state-of-the-art characterization techniques[32,33].

Furthermore, two recent and also strongly developing sister techniques of ALD are molecular layer deposition (MLD)[34,35] of purely organic films and atomic layer etching (ALE). With the combination of MLD and ALD[36,37] in one growth run, thin film materials were extended to hybrid organic-inorganics which possess a higher degree of flexibility than the functionality bearing pure inorganic compounds. This is desirable in flexible electronics, magnetics[38], vapor barrier applications[39,40], or lithium based silicon batteries[41], to name a few fields. Atomic layer etching, based on self-limiting etch half-reactions by two or more sequentially supplied gases, holds the promise of better etch uniformity on three dimensional surface topographies as well as on large wafers compared to classic reactive ion etching[42].

The mechanical, electrical and thermal properties of materials in nano- and microscale are determined by their composition, size and morphology. Therefore, the ALD (as well as MLD and ALE) processes require accurate and reliable monitoring and characterization techniques to ensure desired material functionality. In general, an initial state of an ALD process is well-defined as commercial high-purity targets with specified chemical composition are commonly

used. On the other hand, several post-mortem chemical characterization techniques, such as Time-Of-Flight Secondary Ion Mass Spectrometry (TOF-SIMS)[43,44], Scanning Transmission Electron Microscopy[45] combined with Energy-Dispersive X-ray Spectroscopy (STEM/EDX) as well as Atom Probe Tomography (APT)[46], can provide information on chemical structure of deposited thin films in 3D with nanoscale resolution[47–49]. Furthermore, the nanometric depth resolution can be reached with X-ray photoelectron spectroscopy (XPS) but in this case the lateral resolution is in the order of several microns.[50] However, information on chemical reactions and chemical by-products, which occur from the surface reactions between the solid substrates and gas precursors, is much more challenging to assess. Late detection of deposition failures can have critical economic consequences during mass production of ALD thin films in industry. Although the quality of thin films can be verified with the aforementioned post-mortem techniques, the time required to conduct *ex situ* material characterization, can vary from several hours to several weeks. This mainly results from the demand of performing such measurements under high- or ultrahigh-vacuum (HV and UHV, respectively) conditions, the efficiency of material sputtering with an ion beam (TOF-SIMS) and tedious sample preparation (i.e. lamellas and tips)[51–54] with an additional instrumentation, such as focused ion beam (FIB) in the case of STEM/EDX and APT. Therefore, *in situ* analysis is of particular importance for monitoring the ALD growth characteristics and, consequently the quality of the thin films in real time. So far, this was attempted by using various techniques, such as quartz crystal microbalance (QCM), spectroscopic ellipsometry (SE), Fourier transform infrared spectroscopy (FTIR), optical emission spectroscopy (OES), synchrotron-based X-ray techniques and quadrupole mass spectrometry (QMS)[55]. However, none of these techniques provides complete information on the process chemistry. Furthermore, their operation functionality, reliability of obtained data as well as application scope are usually significantly limited. For example, QCM provides information on the deposited layer thickness. However, in this case deposition rates

have to be known in advance, i.e. additional calibration measurements on sample cross-sections have to be done. Besides, QCM sensors are very sensitive to temperature fluctuations, which can lead to incorrect values of layer growth rates[56,57]. Although SE provides information on optical and electrical properties as well as thicknesses of deposited thin films, the data validity and accuracy is determined by the applied optical modelling[58,59]. FTIR measures vibration modes of molecular bonds in a specimen, and therefore allows for detecting functional groups[60]. On the other hand, atoms and monoatomic ions cannot be detected with FTIR as they do not have chemical bonds, do not vibrate and, consequently, do not absorb infrared radiation. This also implies that noble gases, such as He and Ar, cannot be measured with this technique. Furthermore, homonuclear diatomic molecules, such as N_2 and O_2 do not absorb infrared radiation due to their symmetry[61]. These are significant limitations for studying the chemistry of ALD, and thus processes in the deposition chamber, as N_2 and O_2 gases are the main components of the atmosphere (and help indicating deposition chamber leaks and the vacuum level) and Ar is often used as a process purge gas. OES shows potential for plasma-assisted ALD but allows only electronically-excited species to be studied,[62] meaning that ground species cannot be directly measured. The reported *in situ* synchrotron-based X-ray techniques for monitoring ALD can provide wide range of information (such as roughness, thickness, morphology, crystallinity, etc.),[63] however the complete reconstruction of process chemistry is not possible. Among all above mentioned techniques, QMS seems to have the highest potential for studying ALD process chemistry as it measures mass-to-charge ratio, *m/q*, of ionized species, which allows in principle any type of elements or molecules to be detected. However, in the case of QMS, only one *m/q* can be probed at a given time, which implies either reduced amount of available *m/q* values or low time resolution. Furthermore, for monitoring the process online, the chemical products have to be known prior to the deposition and indicated for the data acquisition. This implies that significant or novel phenomena might not be accessible. So far, *in situ* QMS has

been employed for the identification of surface half-reactions in the thermal Al_2O_3 ALD process[64–66], the plasma Al_2O_3 ALD process[67], GaS and AlS [68,69], Sn as metal[70], TiN[71] and Ti(Al)N[66], α-Fe_2O_3[72], ZnO_2[72], and TiO_2 [73].

In this work, we present the potential of incorporating a time-of-flight mass spectrometry (TOFMS) detector on the ALD chamber for the real-time study of the process chemistry and the verification of the reproducibility of subsequent deposition cycles. Due to the operation principle of TOFMS, i.e. complete mass spectra are acquired at given time intervals, all generated ions and ionized molecules can be detected (i.e. parallel detection). This gives a unique opportunity of correlating the ALD substrates, by-products and products signals with the chemical environment of the deposition chamber (i.e. residual gas signals and signals of purge gases). Furthermore, since the TOFMS data is collected *in situ* during the ALD process, the presented solution can be used for immediate quality control of deposited thin films. Consequently, the deposition parameters, such as precursor temperature, pulse and purge duration, etc., can be adjusted promptly to ensure the designed architecture of the chemical structure and process parameters. To the best of our knowledge, the successful application of TOFMS for *in situ* ALD has never been reported before. The presented various types of data analysis approaches show broad potential of TOFMS technique and can also serve as guidelines for monitoring other deposition techniques (such as CVD, MLD and ALE). Furthermore, using *in situ* TOFMS can help improving fundamental process understanding of current hot topics in the field of ALD, such as spatial ALD[74,75] (SALD, which requires high data acquisition frequency), selective ALD[76–78] (demanding low concentration detection) and nanoparticle powder ALD[79–81].

Therefore, TOFMS is expected play a dominant role in the field of *in situ* process monitoring in the near future as it can be used in basic research (especially in material science and nanotechnologies) as well as industrial production lines of functional nano- and micro-devices.

EXPERIMENTAL

Materials

As mentioned, to the best of our knowledge, TOFMS has never been used before for studying ALD processes *in situ*. Therefore, the first measurements were conducted using trimethylaluminium, $Al(CH_3)_3$ (TMA, 98 % purity, from Strem) and DI H_2O as these two gas precursors are commonly used for depositing Al_2O_3, a model ALD system. The chemistry of this process has been broadly analysed in numerous studies (the overview can be found in ref.[9]) and served for the evaluation of results presented in this work. Both precursors were delivered at room temperature to the deposition chamber and 99.9995 % purity argon (from Air Liquide) was used as the purging gas.

Methods

The ALD process was performed using a novel compact cluster system, SC-1 (from Swiss Cluster AG, Thun, Switzerland), which combines ALD and PVD, and therefore enables fabricating films with thicknesses varying from sub-monolayers to thousands of monolayers as well as complex multilayer structures without breaking vacuum between subsequent ALD and PVD depositions.

In this study, only the ALD module of the SC-1 was used. The ALD chamber was connected to a semiconductor graded double-stage screw pump, iH600 (from Edwards Vacuum, Burgess Hill, United Kingdom), which has 600 m^3/h pumping speed and demands about 40 l/min of N_2. The substrate temperature was set to 120°C. The experiment consisted of 20 ALD cycles. Each cycle included 50 ms pulse of TMA and a 30 ms pulse of H_2O without Ar carrier gas, aiming that only the gases of interest are introduced to the chamber. Unconventionally, the Ar flow was stopped during pulsing the precursors (i.e. 250 ms before opening the precursor valve; the

Ar flow was initiated 50 ms after closing the precursor valve) to prevent further pressure increase in the chamber and towards the TOFMS detector. It was also expected that this procedure could provide better precursor efficiency as well as clearer mass spectra during the pulsing time. However, the experiments can be also conducted in a standard flow-mode by modulating the pressure towards TOFMS, and therefore reducing the Ar signal. Between the gas precursor pulses, a 50 cm^3/min (sccm) argon gas purge over 30 s was provided.

The ALD process chemistry was monitored using a process gas analysis TOFMS (pgaTOF, model R with mass resolving power $R = m/\Delta m = 4000$, according to the instrument specification) from TOFWERK AG (Thun, Switzerland), consisting of an electron ionization (EI) ion source (equipped with an open configuration single-channel ion chamber), an orthogonal extraction system, single reflectron TOF analyzer (HTOF) and a multichannel plate (MCP) electron multiplier (from Photonis, USA). The modular structure of the SC-1 allowed the ALD process chamber to be directly connected with the TOFMS ionization chamber using a stainless steel tube mounted on a KF-25 flange of the SC-1, close to the substrate holder. The flow of analytes to the TOFMS was adjusted using a manual leak valve connected to the metallic tube. To avoid long response times of TOFMS to the dynamics of the ALD process, which can be potentially caused by the large dead volume of the metallic tube, an additional pump was provided. This enabled for a flow increase of the analysed ALD process gas in the connecting tube, which was set to approx. 4 sccm by a fixed aperture mounted on the inlet flange of the TOFMS ionizer chamber. The TOFMS was equipped with an ion guide/filter directing the ionized atoms and molecules from the ion source to the TOF analyser. The use of a high-pass filter allowed for selecting the lower threshold of ion transmission. Furthermore, the applied filter comprised notching technology, which allowed a user to attenuate ions of a selected mass from entering the HTOF analyzer. In this work only the ions with 14 Th < m/q < 590 Th were measured. The

lower threshold on the transmitted ions was set because only species with $m/q > 14$ are of interest in the case of the ALD process of Al_2O_3, and therefore lighter ions were not analysed. The transmitted ions were extracted orthogonally into the HTOF analyzer at 22.9 kHz. A waveform was recorded during each TOF extraction, and 2299 waveforms were averaged to form one mass spectrum. The spectral rate was 10 Hz. The TOFMS was optimized to give maximum sensitivity at average resolving power of $R = 3000$. The ionizer temperature was kept at 280 °C. The ionization energy was set to 70 eV and 0.1 mA emission current was used. The data were recorded in the non-proprietary hierarchical data format (HDF5). The experimental setup is presented in Figure 1.

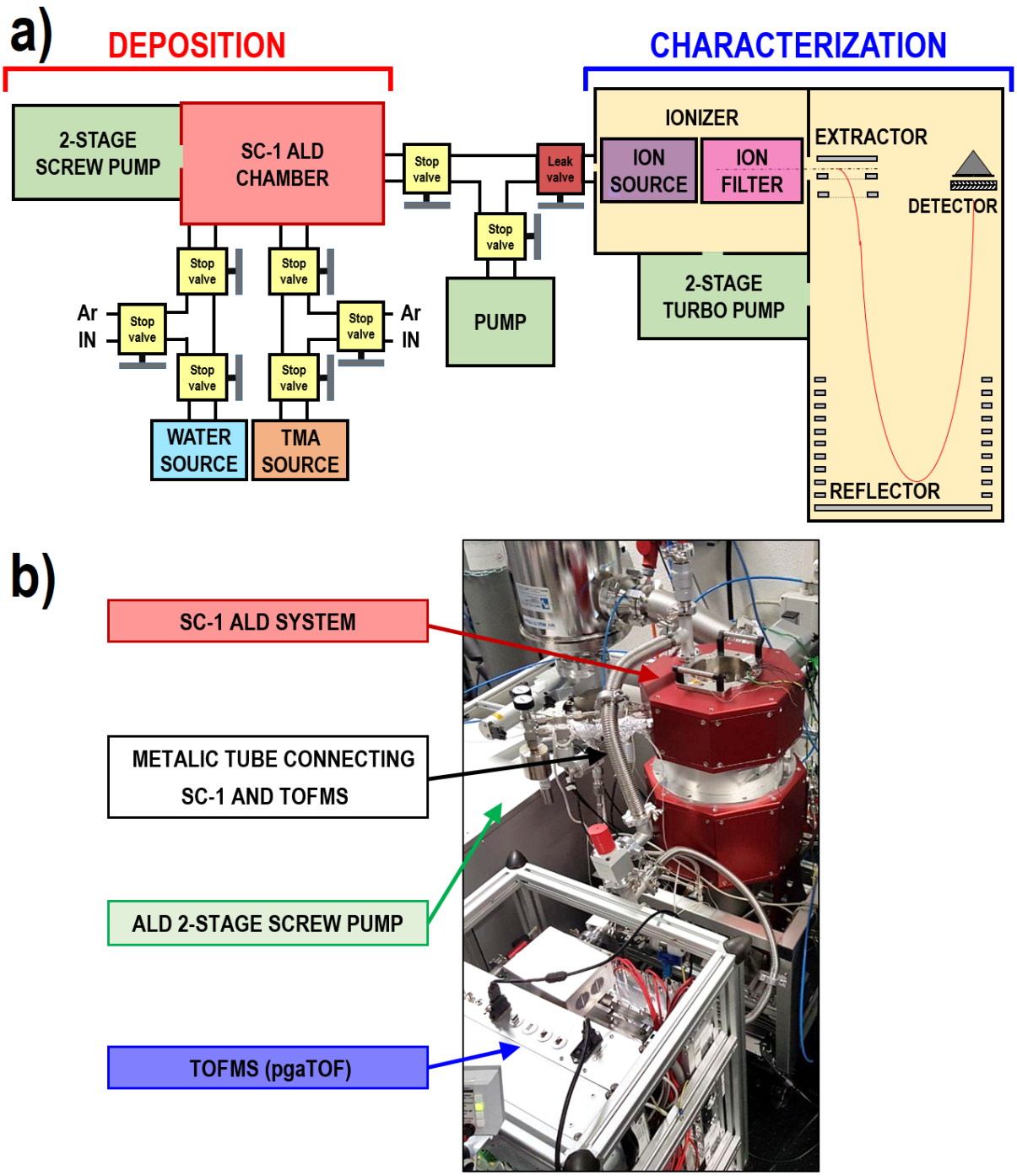

Figure 1. Experimental setup: a) the diagram and b) the picture of ALD+TOFMS system. The ALD process is conducted using the SC-1 (Swiss Cluster, Thun, Switzerland) and the chemical characterization is performed with pgaTOF (TOFWERK, Thun, Switzerland). Description in the text.

RESULTS AND DISCUSSION

In ALD, the surface reactions between the sequentially introduced gas precursors and the surface leads to the release of by-products. The chemistry and amount of these by-products provide an important information regarding the ALD process, from the fundamental understanding of the reaction mechanisms, to the creation of monitoring protocols for reliable and reproducible processes at an industrial scale. The TMA and H_2O process has been extensively studied for the last decades, nevertheless, every so often, there is new information regarding the reaction mechanisms[64,82] that aids to provide a full picture of this complex process. In this work, we study the continuous and parallel detection of all the gas molecules involved at every stage of this process using TOFMS during the TMA-H_2O process (Figure 2).

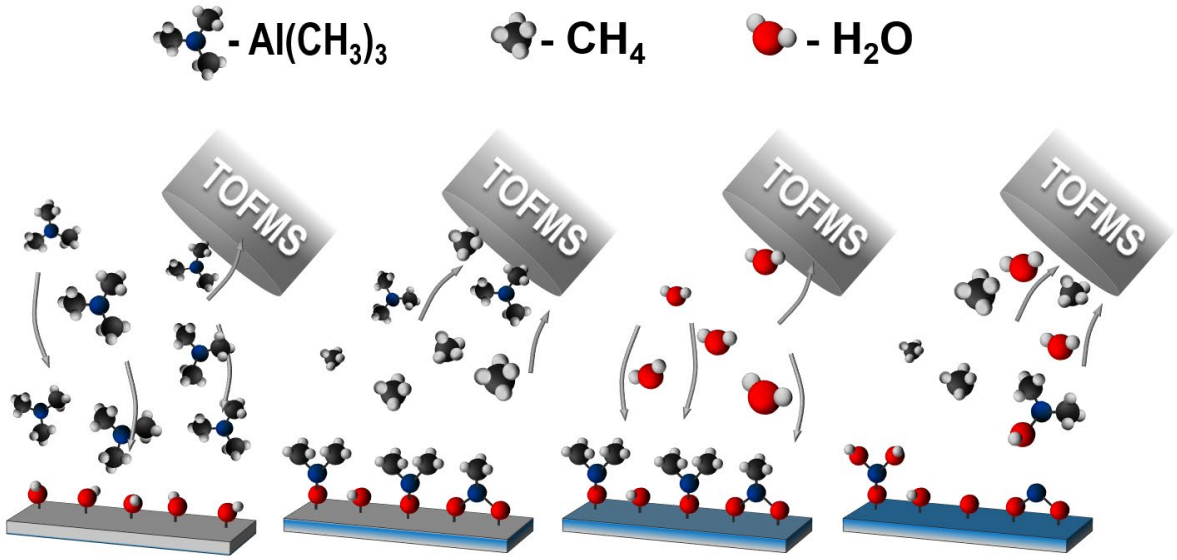

Figure 2. Schematic illustration of a TMA+H_2O deposition process and the parallel detection of all the molecules involved in the process. In this example, TMA reacts with OH sites at the

surface, forming CH_4, and after a purging step, the H_2O reacts with the methyl surface, forming mainly CH_4 in addition to secondary products such as $AlOH(CH_3)_2$.

Parallel detection of all ionized elements and molecules

The main advantage of integrating an *in situ* TOFMS detector with an ALD chamber is the possibility of detecting all light and heavy species as well as simple elements and complex molecules at the same time (parallel detection). Furthermore, the signal evolution of gas precursors, reaction by-products (assuming that their lifetime is longer than the detection speed of the instrument), final products as well as the gases determining the chemical state of the deposition chamber can be monitored easily and directly in real-time. Figure 3 shows the mass spectrum acquired during the entire duration of conducted ALD process consisting of 20 TMA-H_2O cycles and the pump down time of the SC-1 instrument, which aimed at checking the vacuum conditions and the residual gases in the chamber after the deposition. The signal ions were observed in the entire predefined mass spectrum range (i.e. between m/q = 14 Th and 590 Th), proving the detection of simple ions as well as complex ionized molecules. The signal peaks measured at m/q= 72 Th and 18 Th, represent the gas precursors, i.e. $Al(CH_3)_3$ and H_2O, respectively. The peaks observed at m/q = 14 Th, 16 Th, 28 Th, 32 Th and 40 Th are associated with the state of the chamber atmosphere, i.e. N (and/or CH_2), O (and/or CH_4), N_2, O_2 and Ar (purge gas), respectively. As mentioned, the latter one is a great advantage over FTIR spectroscopy, which does not allow single atoms/ions as well as molecules composed of two identical atoms (N_2 and O_2) to be detected. It is worth mentioning that N-related signal peaks (such as ^{14}N, $^{14}N_2$, $^{12}C^{14}N$) predominantly originate from the backflow of nitrogen supplied to the ALD double-stage screw pump (see the Experimental section and the results presented in the next section of this paper). The back flow of N-related species from the screw pump is predominant

when there is no Ar flow into the chamber. The back flow, and thus the N-related species, decreases as the Ar mass flow into the chamber increases.

Furthermore, the performed measurements confirm that CH_4 and $AlOH(CH_3)_2$ (peaks at *m/q* = 16 Th and 74 Th, respectively) are reaction by-products from the surface reactions between the gas precursors TMA and H_2O with surface adsorbates. This is consistent with results previously obtained experimentally[66,83,84] or theoretically using density functional theory (DFT) calculation[85–87] and recently by both.[64]

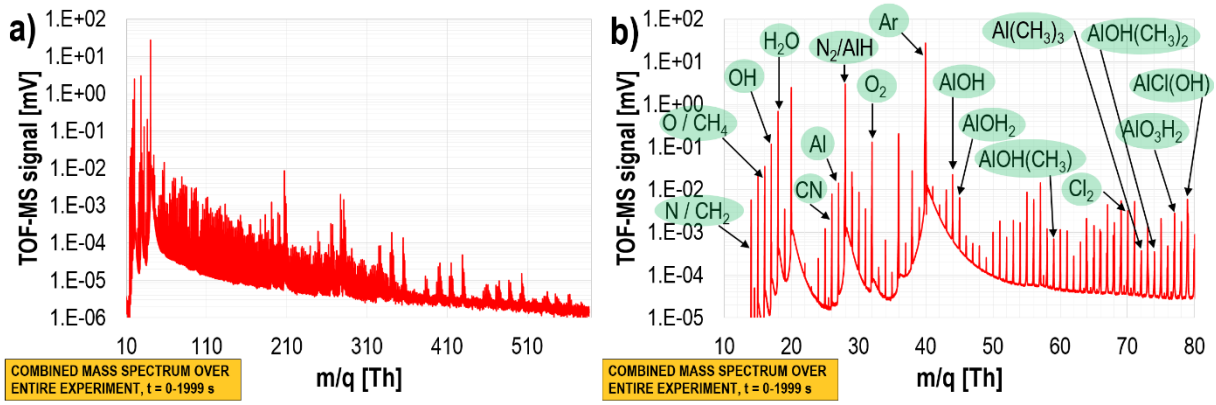

Figure 3. The mass spectrum acquired during the entire ALD process consisting of 20 subsequent series of TMA and H_2O cycles: a) the full measurement range: the strongest signals were observed in the case of process reactants having *m/q* < 290 Th, but heavier ions were also detected, b) a chosen region of mass spectrum with assigned potential reaction substrates and by-products. Note the logarithmic scale.

Monitoring the process chemistry in real time

The simultaneous acquisition of all generated ions during the ALD process allows for tracking the chemistry changes in real time without the necessity of specifying ions of interest (i.e. the ions which have to be known in advance and/or are expected as potential process by-products) prior to a measurement. Furthermore, there are no constraints regarding the number of

analysed ions. These are great advantages of TOFMS over commonly used QMS, which can probe only a limited *m/q* range at the same time and requires defining ions of interest in advance.

In the case of the experiment presented in this study, the dynamics of an ALD Al_2O_3 process (Figure 4) can be characterized based on main signal distributions, which correspond to the TMA and H_2O precursor pulses and corresponding by-products: CH_4 (*m/q* = 16 Th), H_2O (*m/q* = 18 Th) and Al (*m/q* = 27 Th) as well as the purging gas Ar (*m/q* = 40 Th) and N (*m/q* = 14 Th) from the back flow of the N_2 supplied to the pump (this applies to the cases, where a dry pump with N_2 supply is required in the process). Furthermore, the signals of N and H_2O, which do not drop to zero after the end of the ALD process, demonstrate the presence of residual gas in the deposition chamber and/or in the metallic tube connecting the ALD process chamber with TOFMS. Furthermore, as mentioned, the N-containing ions measured during the experiment predominantly come from the backflow of the nitrogen delivered to the vacuum pump. This statement is supported by the distribution of N signal, which always increases when the Ar signal drops (i.e. reduced mass flow of Ar, meaning decreased pressure) between subsequent TMA and H_2O pulses.

In general, monitoring signal evolution in real time can deliver important information on any process deviation from optimal or malfunction induced, for example, by sudden power loss, temperature changes, valve malfunction back flows or gas leaks, which can potentially modify the chemistry of the ALD processes. Divergence between the specified and the actual deposition conditions can have serious consequences, such as undesired contaminations, incorporation of particles in deposited thin films and/or inhomogeneity, different values of growth-per-cycle (GPC), and therefore potentially lead to different mechanical, electrical and thermal properties of the fabricated materials, which ultimately determine their functionality.

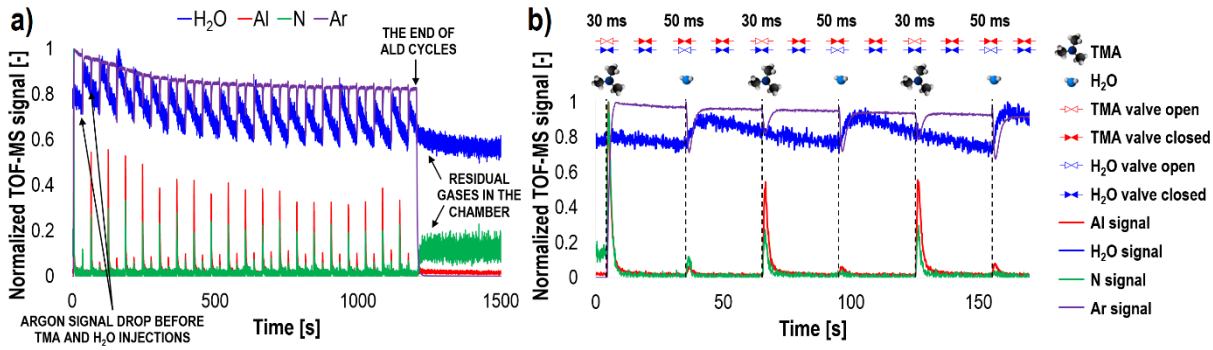

Figure 4. An *in situ* TOFMS integrated within an ALD chamber gives a unique opportunity of monitoring the signal's time evolution of all elements and molecules participating in an ALD process, including products and by-products. The H_2O (blue line) and Al (red line) signals represent the gas precursors, whilst N (green line) and Ar (violet line) signals provide information on the vacuum status of the deposition chamber. The time evolution of the 20-cycle deposition process (a) and magnification of the first three TMA and H_2O cycles (b) are shown. The TOFMS data were normalized to 1 for better visualization. See also Figures 9 to 11.

Another important feature of using *in situ* TOFMS to monitor ALD processes is the possibility of verifying the reproducibility of subsequent cycles, resulting from the amount of delivered gas precursors. Figure 5 shows the characteristic values of ^{27}Al signal distribution, i.e. the ^{27}Al signal peak amplitudes measured, when TMA valve was opened, $S_{Al,max,height@TMA}$ (red points) and their full widths at half maximum (FWHM), $S_{Al,max,width@TMA}$. The variations of these two values indicate that the amount of delivered TMA precursor varied between the cycles. In this case the average value of $S_{Al,max,height@TMA}$ was 1.8±0.2 s (the error was calculated as a standard deviation), which means approx. 11% discrepancy in this case. It is worth mentioning that the significantly higher first Al signal peak results from the very first pulse of TMA. In this case, most likely a larger volume of evaporated gas precursor is delivered compared to the volumes delivered at subsequent pulses, which have less time to re-evaporate the same volume of gas in

between consecutive cycles. Such an observation is one of the first immediate information about the variation in the process in every cycle.

Although the ALD process is self-limiting by definition and the excess of the TMA precursor does not induce an increase of GPC values, its deficiency can prevent achieving the complete substrate surface coverage, especially when coating 3D complex geometries, as every cycle would gradually increase the surface of the material, and thus increase the required amount of precursor molecules. Furthermore, this can potentially lead to the layer mixing if more than one thin film type is deposited.

The presented type of analysis can be performed for any number of precursors used during the deposition process since mass spectra are acquired continuously and simultaneously using TOFMS. Therefore, complex multilayer structures can be studied easily and efficiently.

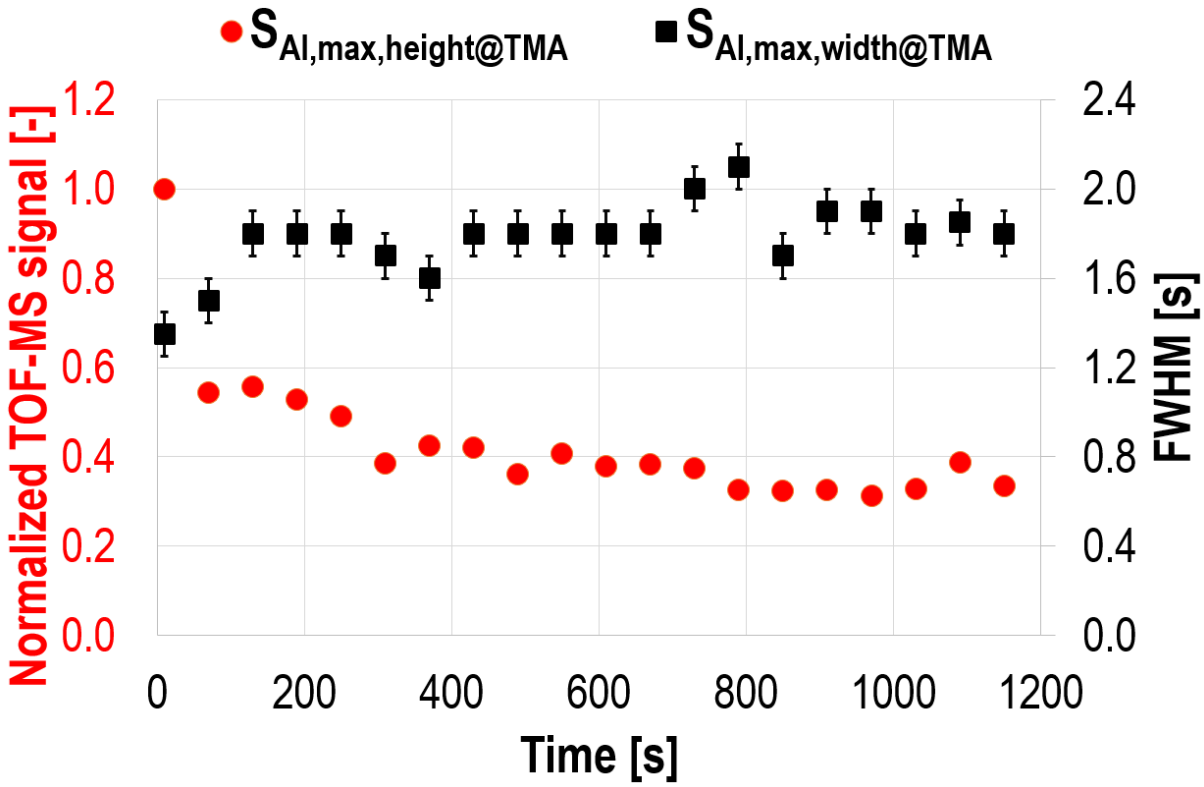

Figure 5. Comparison of Al signal peaks measured during the subsequent TMA injections. The variations of peak height, $S_{Al,max,height@TMA}$, and width, $S_{Al,max,width@TMA}$, values can provide indications on the amount of delivered gas precursor, and therefore the reproducibility of subsequent ALD cycles.

Chemistry comparison of TMA and H_2O pulses

The mass spectra represent the cumulative signal detected during a specified time of an ALD process. Therefore, they are especially useful when the occurrence of specific species has to be verified. This is particularly important in the case of elements, whose amount in a given chemical system is extremely low and/or if their ionization efficiency is insufficient to represent their signal evolution in time. Furthermore, the comparison of mass spectra, which were acquired during two different cycles or two different pulses, can deliver important information on the process chemistry.

Figure 6 shows the signal evolution curves for Al, H_2O and Ar measured during the 10th ALD cycle (i.e. the 10th TMA and the 10th H_2O pulses). These signal peaks were chosen arbitrary in the middle of twenty ALD cycles performed during the experiment as the most representative for the analysis (i.e. they are not biased with the initial state of the ALD process chamber; see the discussion explaining the difference between the 1st cycle and the following ones). Based on the 2 s acquisition time of each peak (marked with beige rectangles in Figure 6a), the corresponding mass spectra were generated for the 10th Al signal peaks measured at TMA and H_2O pulses, $S_{10th\_Al\_peak@TMA}$ and $S_{10th\_Al\_peak@H2O}$, respectively (Figure 6b). Note that the actual TMA pulse lasted 50 ms and H_2O pulse lasted 30 ms (see the Experimental part). Therefore, the given signal values also include the Ar purge time. The most significant differences between the two mass spectra were observed for m/q < 110 Th. The direct comparison (Figure 7a) as well as the

difference between the two curves, $\Delta S = S_{10th\_Al\_peak@TMA} - S_{10th\_Al\_peak@H2O}$, (Figure 7b) reveal significantly higher Ar content in the case of TMA pulse. This was deduced based on the magnitude of peaks measured at m/q = 40 Th and 20 Th, which correspond to $^{40}Ar^{+}$ and $^{40}Ar^{2+}$ ions. This is consistent with the fact that more Ar is injected to the chamber during TMA pulses as the valve of TMA is opened for a longer time than in the case of H_2O valve. Furthermore, most of the complex ions generated during the ALD process were generated within the TMA pulse, i.e. basically only the CH_4 (m/q = 16 Th) as well as $^{1}H^{16}O^{+}$ and $^{1}H_2{}^{16}O^{+}$ ions (m/q = 17 Th and 18 Th) were observed during the H_2O pulse. This is consistent with the reaction mechanisms of TMA and H_2O with surface adsorbates[88] (see in the following sections of this paper).

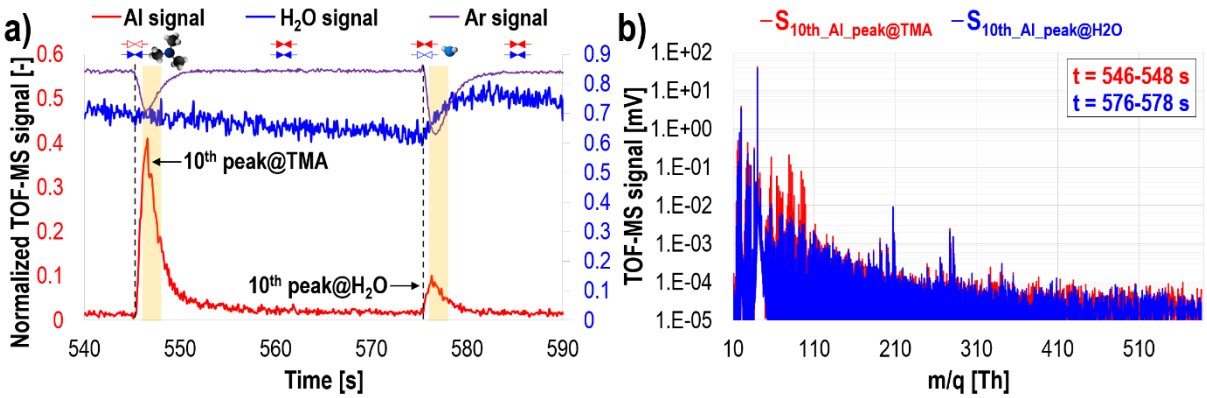

Figure 6. Results for the 10th TMA and 10th H_2O pulses: a) the signals of two subsequent pulses were integrated over 2s of acquisition time (marked with beige rectangles) and b) the generated mass spectra (note the logarithmic scale).

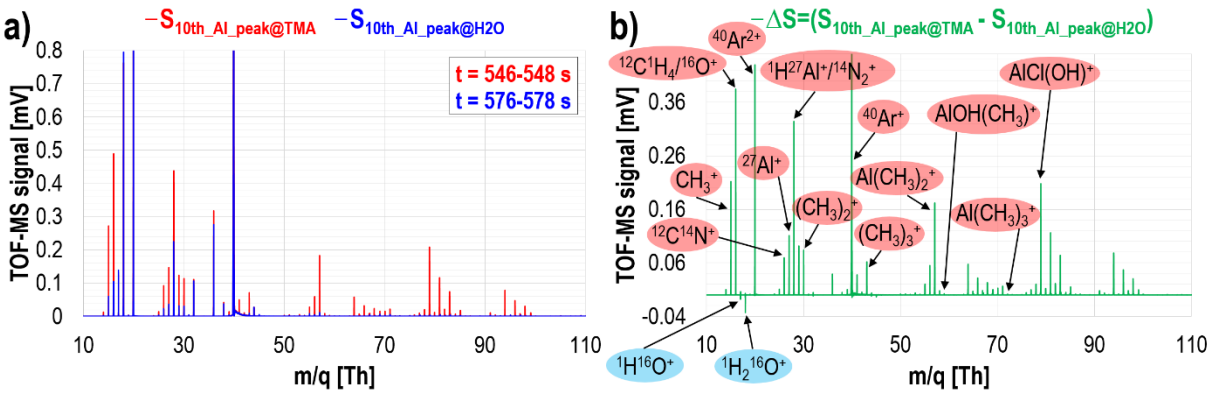

Figure 7. Comparison of mass spectra obtained at the 10th TMA (red line) the 10th H_2O (blue line) pulses (a) and their difference, ΔS, (b) within mass range between 10 Th and 110 Th. The ions dominantly generated during the 10th TMA pulse are marked with red circles and the ions dominantly generated during the 10th H_2O pulse are marked with blue circles.

The presented comparison of mass spectra can be obtained for any step of the deposition process. Therefore, it can serve for studying the chemistry at different timescales as well as for validating the reproducibility and quality of the implemented protocols.

High mass resolution of TOFMS

The acquisition of ions having the same or very similar *m/q* values, is one of the major challenges of mass spectrometry due to the potential mass interference.[32,33,89] However, providing sufficiently high mass resolution of a detector, many isobaric ions can be distinguished.

The nominal mass peak in a mass spectrum, represents a signal integrated over a $m/q \pm 0.5$ Th range. This means that ions of more than one element/molecule can contribute to the total measured signal. For example, the signal measured at m/q = 16 Th can be potentially associated with $^{16}O^+$ and $^{12}C^1H_4^+$ ions at m/q = 15.995 Th and 16.031 Th, respectively. The m/q difference between $^{16}O^+$ and $^{12}C^1H_4^+$ ions is $\Delta m_{CH4\text{-}O} = 3.6\times10^{-2}$ Th, which means that the detector's mass resolving power of approximately $R = m/\Delta m = 444$ Th/Th is required to distinguish them. This value is far below the TOFMS mass resolution specified by the manufacturer (i.e. $m/\Delta m = 4000$ Th/Th) and, indeed, in the mass range 15.5 Th - 16.5 Th, two distinct signal peaks were measured (Figure 8). Furthermore, the significant difference between the amount of detected ^{16}O and $^{12}C^1H_4$ ions in the case of TMA and H_2O pulses can be observed. In the case of the 10th ALD

cycle, approximately 4 times more $^{12}C^{1}H_4$ ions were detected during the TMA pulse compared to the H_2O pulse. The estimation of ^{16}O ions is more difficult to assess as its signal peak overlaps with the tail of $^{12}C^{1}H_4$ signal peak in the case of TMA. Figure 9 shows the signal evolution of the ions measured at nominal m/q = 16 Th, ^{16}O ions and $^{12}C^{1}H_4$ ions. The data suggest that $^{12}C^{1}H_4$ ions are produced during both, TMA and H_2O pulses.

The distinction between ^{16}O and $^{12}C^{1}H_4$ ions is particularly important for understanding the ALD Al_2O_3 process because the main by-product $^{12}C^{1}H_4$, present in both TMA and H_2O pulses, determines the surface coverage reached in each pulse. Furthermore, the possible contribution of ^{16}O, either by the process itself or a leak from the atmosphere, can interfere with the analysis if both peaks are taken into account as one.

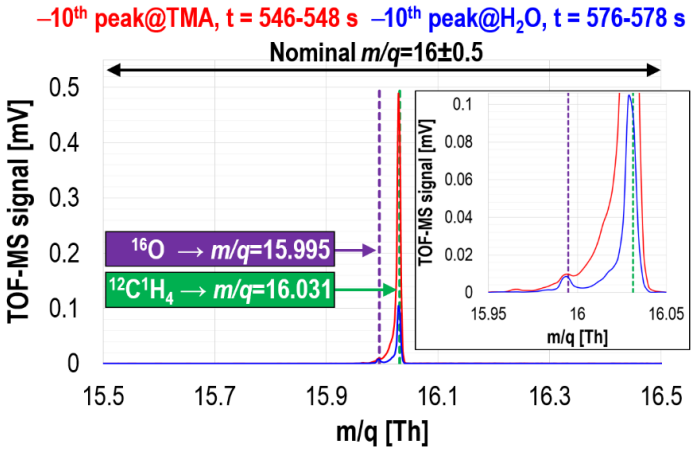

Figure 8. High mass resolution of TOFMS detector allows for distinguishing $^{12}C^{1}H_4^{+}$ ion from $^{16}O^{+}$ ion signals. The curves measured for the 10th ALD cycle are shown: the red and blue lines represent data measured at the 10th TMA pulse and the 10th H_2O pulse, respectively.

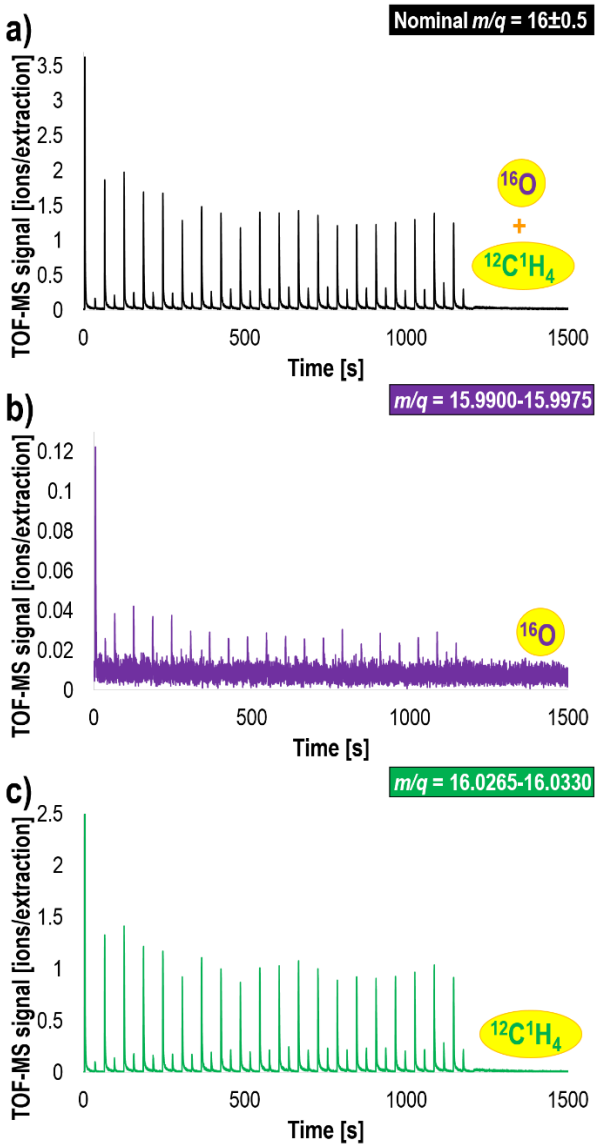

Figure 9. Signal evolution of the ions measured at nominal m/q = 16 Th (a), $^{16}O^+$ ions (b) and $^{12}C^1H_4^+$ ions (c). In the case of $^{16}O^+$ and $^{12}C^1H_4^+$ signals, the signal integration ranges were chosen based on the full width at half maximum (FWHM) of the two peaks presented in Figure 8. Note different scales.

Detection of TMA+H_2O process products

The surface reactions in the ALD deposition process of Al_2O_3 have been studied in more detail in previous reports[66,83,84]. According to these works and focusing only on the formation of by-products, a TMA molecule reaching the OH-terminated surface reacts as follows:

$$xOH\ (s) + Al(CH_3)_3\ (g) \rightarrow O_xAl(CH_3)_{3-x}\ (s) + xCH_4\ (g) \quad (1)$$

with x=1, 2 or 3. Subsequently, the second half-reaction with H_2O, when x=1 or 2, yields

$$O_xAl(CH_3)_{3-x}\ (s) + (3-x)H_2O\ (g) \rightarrow O_xAl(OH)_{3-x}\ (s) + (3-x)CH_4\ (g) \quad (2)$$

The main reaction product of both surface reactions is methane (CH_4). Furthermore, Werbrouck et al.[64] have also identified a secondary reaction product during the water cycle, the volatile $HOAl(CH_3)_2$ with m/q = 74 Th, using *in situ* quadrupole mass spectrometry. The reaction pathway to the formation of that compound, was not completely revealed. However, the performed density functional theory (DFT) calculations suggest cooperative effects of multiple Al-CH_3 surface groups to dissociate energetically favourably the impinging H_2O molecule and to supply the OH hydroxyl group to form volatile $HOAl(CH_3)_2$.

A distinct peak at m/q = 74 Th, corresponding to $HOAl(CH_3)_2$ was also observed in the mass spectrum measured using *in situ* TOFMS in our study (Figure 3b). Furthermore, we observed also a strong signal peak at m/q = 59 Th, representing $HOAl(CH_3)$ ions, whose signal evolution in time shows a strong correlation with Al signal distribution (Figure 10). In this case, the locations of signal maxima for Al and $HOAl(CH_3)$ ions appear at the same time and correspond to the TMA pulses. This observation can potentially indicate other cooperative mechanisms leading to volatile Al molecules during the TMA pulse similar to the one proposed by Werbrouck et al.[64] during the water pulse and can be potentially responsible for the carbon contamination in Al_2O_3 ALD deposits.

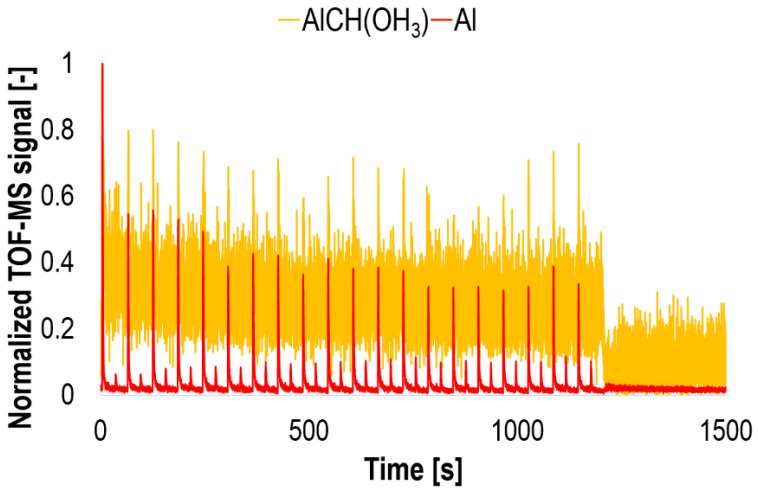

Figure 10. Signal evolution of the expected TMA+H_2O process products: $HOAl(CH_3)$ (*m/q* = 59 Th; the orange line) signal compared to the Al (*m/q* = 27 Th; the red line) signal. Data normalized to 1 for better comparison.

High sensitivity of TOFMS: detection and accurate assignment of contaminants

The presence of contaminants in the deposition system constitutes an important issue in the case of thin film fabrication as they can affect the ultimate properties of designed chemical systems, especially in semiconductor industry where contaminant doping can drastically change electrical film properties. The most common contaminants usually come from the deposition chamber (for example, debris of the precursors used previously in the same reactor), substrates (for example, inappropriate storage, cleaning and/or handling of wafers), process gas precursors (decomposition or impurities) or purge gases. In the mass spectrum presented in Figure 3, various distinct peaks, which cannot be directly associated with TMA and H_2O by-products, were measured. One of them was observed at *m/q* = 79 Th. Knowing that the TMA precursor can contain trace amount of Cl contamination (due to the synthesis process of TMA)[88], in conjunction with a detailed comparative analysis of different signal evolutions allowed assigning this *m/q* value to AlCl(OH) ions (Figure 11). This is confirmed by the signal distribution at *m/q* = 96 Th, which corresponds to $AlCl(OH)_2$ ions.

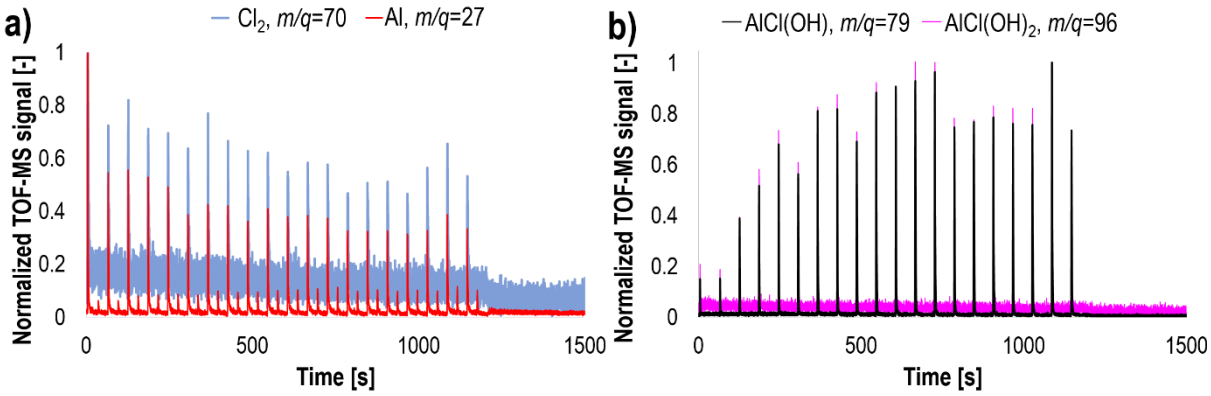

Figure 11. Detection of trace contaminants. The presence of Cl_2 ions in the deposition chamber was measured with TOFMS. Furthermore, the Cl_2 signal peaks correspond to the TMA pulses, i.e. are not observed during H_2O pulses (a). Signal evolution at m/q = 79 Th (black line) was assigned to AlCl(OH) ions. This was confirmed by the comparable signal distribution of $AlCl(OH)_2$ ions (m/q = 96 Th, pink line) (b). Data normalized to 1 for better comparison.

CONCLUSIONS

Due to their extraordinary mechanical, electrical, magnetic and optical properties, sub-nanometric and sub-micrometric thin films attract a lot of attention in many fields, such as microelectronics, nanotechnology, biotechnology, medicine and others. Since the ultimate functionality of thin films is determined by their chemical structure, appropriate and reliable process monitoring techniques are demanded to ensure efficient fabrication of high-quality materials. This is particularly important in the case of massive industrial production lines, where any process failures can have serious financial consequences.

As presented in this work, integrating *in situ* TOFMS with an ALD system allows for parallel detection of all ionized molecule fragments including the ionized parent molecules in real time. Therefore, any process deviation from optimal or malfunction can be detected at an early stage, and consequently the deposition parameters, such as precursor temperature, pulse duration and

pressure in the deposition chamber can be corrected immediately to ensure deposition of the intended architecture of the chemical structure. Furthermore, many of the downsides of the other commonly used *in situ* techniques (such as QCM, FTIR and QMS) are overcome when using TOFMS. This seems to make it superior for monitoring most thin film deposition processes as the there are no limitations on the number of analyzed species and their type (single ions or ionized molecules), the data acquisition is fast, non-intrusive and representative for the entire deposition system (i.e. not limited to a small local surface fraction). Furthermore, the chemical information is obtained directly, whilst other techniques often require dedicated calibration procedures (for example usefulness of QCM measurements are determined by the knowledge on deposition rates). However, despite the impressive potential of TOFMS, the problem of distinguishing actual process by-products and products from the post-ionized species remains an important issue. This can make studying the chemistry of novel thin films difficult, and therefore theoretical models as well as advanced simulations are required for basic science. Furthermore, to evaluate the final thicknesses of the deposited layers either complementary techniques should be used together with TOFMS or specific methodology, which allow the saturation levels to be recognized, should be developed.

Another important issues of combining *in situ* TOFMS with ALD are process kinetics and process mechanisms. In general, TOFMS allows complete mass spectra to be acquired at very high rates, i.e. 1 kHz in a standard acquisition mode (this value can be much higher under dedicated operation conditions). However, in our experimental setup, we opted for a non-invasive configuration (preferred for a production setting) where the analyser is outside the ALD reactor with appropriate flow restrictive hardware interface (bellow, valve, and apertures) to control its input pressure. As such, TOFMS measurements capture the time scale of the system response, which is composed of the surface reaction time, the transport of molecules to the surface and the transport of reaction products to the TOFMS.

In an ALD system gases react with all surfaces in the chambers and tubes. Therefore, during our measurements we tried to keep the same temperature of the substrate, chamber walls and the tube connecting the ALD chamber with TOFMS. However, using the current setup for evaluating a percentage of the reaction gases coming only from a sample surface and decoupling the influences of other surfaces require additional dedicated experiments. This can be potentially achieved, for example, by measuring TOFMS signal changes when varying sample temperature (and keeping constant temperatures of other surfaces) and/or by significantly increasing the surface area of the substrate by incorporating nanoparticles or nanotubes and comparing the results to those obtained for a flat surface. The complexity of kinetics and process mechanisms are too detailed and far beyond the scope of this work but they will be addressed in our further investigations. Furthermore, it is worth mentioning that the TOFMS instrument can be configured to allow for direct connection of the analyser to any reaction chamber.

While this paper clearly demonstrates the usefulness of *in situ* TOFMS analysis in an ALD process, it is also expected that the same could apply to other deposition techniques such as chemical vapour deposition as well as its plasma enhanced variants, and etch applications for process optimization, monitoring and control with the important characteristic that end point detection could be implemented for complex interfaces such as transitions involving binary, ternary and quaternary alloys. Furthermore, the high acquisition speed will be particularly critical for sources operating in pulsed modes and processes involving deposition and etch of nanolayered stacks.

Finally, the methods of analysing the TOFMS data presented in this work can serve as guidelines for verifying the reproducibility of subsequent deposition cycles, recognition of potential contaminants and judging on the thin film fabrication quality.

FUNDING SOURCES

The authors have no funding information to declare.

REFERENCES

(1) Ritala, M.; Leskelä, M. Chapter 2 - Atomic Layer Deposition. In *Handbook of Thin Films*; Singh Nalwa, H. B. T.-H. of T. F., Ed.; Academic Press: Burlington, 2002; pp 103–159. https://doi.org/https://doi.org/10.1016/B978-012512908-4/50005-9.

(2) Martin, P. M. *Handbook of Deposition Technologies for Films and Coatings: Science, Applications and Technology*, 3rd ed.; Elsevier: Oxford, UK, 2010.

(3) Stefik, M.; Cornuz, M.; Mathews, N.; Hisatomi, T.; Mhaisalkar, S.; Grätzel, M. Transparent, Conducting Nb:SnO 2 for Host-Guest Photoelectrochemistry. *Nano Lett.* **2012**, *12* (10), 5431–5435. https://doi.org/10.1021/nl303101n.

(4) Bakke, J. R.; Pickrahn, K. L.; Brennan, T. P.; Bent, S. F. Nanoengineering and Interfacial Engineering of Photovoltaics by Atomic Layer Deposition. *Nanoscale* **2011**, *3* (9), 3482–3508. https://doi.org/10.1039/c1nr10349k.

(5) Johnson, R. W.; Hultqvist, A.; Bent, S. F. A Brief Review of Atomic Layer Deposition: From Fundamentals to Applications. *Mater. Today* **2014**, *17* (5), 236–246. https://doi.org/10.1016/j.mattod.2014.04.026.

(6) Puurunen, R. L. Surface Chemistry of Atomic Layer Deposition: A Case Study for the Trimethylaluminum/Water Process. *J. Appl. Phys.* **2005**, *97* (12). https://doi.org/10.1063/1.1940727.

(7) Profijt, H. B.; Potts, S. E.; van de Sanden, M. C. M.; Kessels, W. M. M. Plasma-Assisted

Atomic Layer Deposition: Basics, Opportunities, and Challenges. *J. Vac. Sci. Technol. A Vacuum, Surfaces, Film.* **2011**, *29* (5), 050801. https://doi.org/10.1116/1.3609974.

(8) Knez, M.; Nielsch, K.; Niinistö, L. Synthesis and Surface Engineering of Complex Nanostructures by Atomic Layer Deposition. *Adv. Mater.* **2007**, *19* (21), 3425–3438. https://doi.org/10.1002/adma.200700079.

(9) George, S. M. Atomic Layer Deposition: An Overview. *Chem. Rev.* **2010**, *110* (1), 111–131. https://doi.org/10.1021/cr900056b.

(10) Marichy, C.; Bechelany, M.; Pinna, N. Atomic Layer Deposition of Nanostructured Materials for Energy and Environmental Applications. *Adv. Mater.* **2012**, *24* (8), 1017–1032. https://doi.org/10.1002/adma.201104129.

(11) Niinistö, L.; Päiväsaari, J.; Niinistö, J.; Putkonen, M.; Nieminen, M. Advanced Electronic and Optoelectronic Materials by Atomic Layer Deposition: An Overview with Special Emphasis on Recent Progress in Processing of High-k Dielectrics and Other Oxide Materials. *Phys. Status Solidi Appl. Res.* **2004**, *201* (7), 1443–1452. https://doi.org/10.1002/pssa.200406798.

(12) Puurunen, R. L.; Saarilahti, J.; Kattelus, H. Implementing ALD Layers in MEMS Processing. **2007**, 3–14. https://doi.org/10.1149/1.2779063.

(13) Puurunen, R. L.; Kattelus, H.; Suntola, T. *Atomic Layer Deposition in MEMS Technology*; Elsevier Inc, 2010. https://doi.org/10.1016/B978-0-8155-1594-4.00026-7.

(14) Davidson, B. D.; Chang, Y. J.; Seghete, D.; George, S. M.; Bright, V. M. Atomic Layer Deposition (ALD) Tungsten Nems Devices via a Novel Top-down Approach. *Proc. IEEE Int. Conf. Micro Electro Mech. Syst.* **2009**, 120–123.

https://doi.org/10.1109/MEMSYS.2009.4805333.

(15) Sterner, J.; Malmström, J.; Stolt, L. Study on ALD In2S3/Cu(In, Ga)Se2 Interface Formation. *Prog. Photovoltaics Res. Appl.* **2005**, *13* (3), 179–193. https://doi.org/10.1002/pip.595.

(16) Platzer-Björkman, C.; Lu, J.; Kessler, J.; Stolt, L. Interface Study of CuInSe2/ZnO and Cu(In,Ga)Se2/ZnO Devices Using ALD ZnO Buffer Layers. *Thin Solid Films* **2003**, *431–432* (03), 321–325. https://doi.org/10.1016/S0040-6090(03)00229-3.

(17) Kobayashi, T.; Kumazawa, T.; Jehl Li Kao, Z.; Nakada, T. Cu(In,Ga)Se2 Thin Film Solar Cells with a Combined ALD-Zn(O,S) Buffer and MOCVD-ZnO:B Window Layers. *Sol. Energy Mater. Sol. Cells* **2013**, *119*, 129–133. https://doi.org/10.1016/j.solmat.2013.05.052.

(18) Naghavi, N.; Abou-Ras, D.; Allsop, N.; Barreau, N.; Bücheler, S.; Ennaoui, A.; Fischer, C. H.; Guillen, C.; Hariskos, D.; Herrero, J.; Klenk, R.; Kushiya, K.; Lincot, D.; Menner, R.; Nakada, T.; Platzer-Björkman, C.; Spiering, S.; Tiwari, A. N.; Törndahl, T. Buffer Layers and Transparent Conducting Oxides for Chalcopyrite Cu(In,Ga)(S,Se)2 Based Thin Film Photovoltaics: Present Status and Current Developments. *Prog. Photovoltaics Res. Appl.* **2010**, *18* (6), 411–433. https://doi.org/10.1002/pip.955.

(19) Williams, V. O.; Jeong, N. C.; Prasittichai, C.; Farha, O. K.; Pellin, M. J.; Hupp, J. T. Fast Transporting ZnO-TiO 2 Coaxial Photoanodes for Dye-Sensitized Solar Cells Based on ALD-Modified SiO 2 Aerogel Frameworks. *ACS Nano* **2012**, *6* (7), 6185–6196. https://doi.org/10.1021/nn3015695.

(20) Clark, M. D.; Jespersen, M. L.; Patel, R. J.; Leever, B. J. Ultra-Thin Alumina Layer Encapsulation of Bulk Heterojunction Organic Photovoltaics for Enhanced Device

Lifetime. *Org. Electron.* **2014**, *15* (1), 1–8. https://doi.org/10.1016/j.orgel.2013.10.014.

(21) Wu, J.; Fei, F.; Wei, C.; Chen, X.; Nie, S.; Zhang, D.; Su, W.; Cui, Z. Efficient Multi-Barrier Thin Film Encapsulation of OLED Using Alternating Al2O3 and Polymer Layers. *RSC Adv.* **2018**, *8* (11), 5721–5727. https://doi.org/10.1039/c8ra00023a.

(22) Park, S. H. K.; Oh, J.; Hwang, C. S.; Lee, J. I.; Yang, Y. S.; Chu, H. Y. Ultrathin Film Encapsulation of an OLED by ALD. *Electrochem. Solid-State Lett.* **2005**, *8* (2), 21–24. https://doi.org/10.1149/1.1850396.

(23) Park, J. S.; Chae, H.; Chung, H. K.; Lee, S. I. Thin Film Encapsulation for Flexible AM-OLED: A Review. *Semicond. Sci. Technol.* **2011**, *26* (3). https://doi.org/10.1088/0268-1242/26/3/034001.

(24) Choi, D. won; Park, J. S. Highly Conductive SnO2 Thin Films Deposited by Atomic Layer Deposition Using Tetrakis-Dimethyl-Amine-Tin Precursor and Ozone Reactant. *Surf. Coatings Technol.* **2014**, *259* (PB), 238–243. https://doi.org/10.1016/j.surfcoat.2014.02.012.

(25) Yamada, A.; Sang, B.; Konagai, M. Atomic Layer Deposition of ZnO Transparent Conducting Oxides. *Appl. Surf. Sci.* **1997**, *112*, 216–222. https://doi.org/10.1016/S0169-4332(96)01022-7.

(26) Abb, M.; Sepúlveda, B.; Chong, H. M. H.; Muskens, O. L. Transparent Conducting Oxides for Active Hybrid Metamaterial Devices. *J. Opt. (United Kingdom)* **2012**, *14* (11). https://doi.org/10.1088/2040-8978/14/11/114007.

(27) Otto, M.; Kroll, M.; Käsebier, T.; Lee, S. M.; Putkonen, M.; Salzer, R.; Miclea, P. T.; Wehrspohn, R. B. Conformal Transparent Conducting Oxides on Black Silicon. *Adv.*

Mater. **2010**, *22* (44), 5035–5038. https://doi.org/10.1002/adma.201002515.

(28) Daubert, J. S.; Hill, G. T.; Gotsch, H. N.; Gremaud, A. P.; Ovental, J. S.; Williams, P. S.; Oldham, C. J.; Parsons, G. N. Corrosion Protection of Copper Using Al2O3, TiO2, ZnO, HfO2, and ZrO2 Atomic Layer Deposition. *ACS Appl. Mater. Interfaces* **2017**, *9* (4), 4192–4201. https://doi.org/10.1021/acsami.6b13571.

(29) Härkönen, E.; Kolev, I.; Díaz, B.; Światowska, J.; Maurice, V.; Seyeux, A.; Marcus, P.; Fenker, M.; Toth, L.; Radnoczi, G.; Vehkamäki, M.; Ritala, M. Sealing of Hard CrN and DLC Coatings with Atomic Layer Deposition. *ACS Appl. Mater. Interfaces* **2014**, *6* (3), 1893–1901. https://doi.org/10.1021/am404906x.

(30) Guerra-Nuñez, C.; Park, H. G.; Utke, I. Atomic Layer Deposition for Surface and Interface Engineering in Nanostructured Photovoltaic Devices. *At. Layer Depos. Energy Convers. Appl.* **2017**, 119–148. https://doi.org/10.1002/9783527694822.ch4.

(31) Skoog, S. A.; Elam, J. W.; Narayan, R. J. Atomic Layer Deposition: Medical and Biological Applications. *Int. Mater. Rev.* **2013**, *58* (2), 113–129. https://doi.org/10.1179/1743280412Y.0000000009.

(32) Priebe, A.; Pethö, L.; Huszár, E.; Xie, T.; Utke, I.; Michler, J. High Sensitivity of Fluorine Gas-Assisted FIB-TOF-SIMS for Chemical Characterization of Buried Sublayers in Thin Films. *ACS Appl. Mater. Interfaces* **2021**. https://doi.org/10.1021/acsami.1c01627.

(33) Priebe, A.; Huszar, E.; Nowicki, M.; Pethö, L.; Michler, J. Mechanisms of Fluorine-Induced Separation of Mass Interference during TOF-SIMS Analysis. *Anal. Chem.* **2021**. https://doi.org/10.1021/acs.analchem.1c01661.

(34) Yoshimura, T.; Tatsuura, S.; Sotoyama, W. Polymer Films Formed with Monolayer Growth Steps by Molecular Layer Deposition. *Appl. Phys. Lett.* **1991**, *59* (4), 482–484. https://doi.org/10.1063/1.105415.

(35) Zhou, H.; Bent, S. F. Fabrication of Organic Interfacial Layers by Molecular Layer Deposition: Present Status and Future Opportunities. *J. Vac. Sci. Technol. A Vacuum, Surfaces, Film.* **2013**, *31* (4), 040801. https://doi.org/10.1116/1.4804609.

(36) George, S. M.; Dameron, A. A.; Yoon, B. Surface Chemistry for Molecular Layer Deposition of Organic and Hybrid Organic-Inorganic Polymers. *Acc. Chem. Res.* **2009**, *42* (4), 498–508. https://doi.org/10.1021/ar800105q.

(37) Meng, X. An Overview of Molecular Layer Deposition for Organic and Organic-Inorganic Hybrid Materials: Mechanisms, Growth Characteristics, and Promising Applications. *J. Mater. Chem. A* **2017**, *5* (35), 18326–18378. https://doi.org/10.1039/c7ta04449f.

(38) Philip, A.; Niemelä, J. P.; Tewari, G. C.; Putz, B.; Edwards, T. E. J.; Itoh, M.; Utke, I.; Karppinen, M. Flexible ϵ-Fe2O3-Terephthalate Thin-Film Magnets through ALD/MLD. *ACS Appl. Mater. Interfaces* **2020**, *12* (19), 21912–21921. https://doi.org/10.1021/acsami.0c04665.

(39) Xiao, W.; Hui, D. Y.; Zheng, C.; Yu, D.; Qiang, Y. Y.; Ping, C.; Xiang, C. L.; Yi, Z. A Flexible Transparent Gas Barrier Film Employing the Method of Mixing ALD/MLD-Grown Al2O3 and Alucone Layers. *Nanoscale Res. Lett.* **2015**, *10* (1). https://doi.org/10.1186/s11671-015-0838-y.

(40) Chen, Z.; Wang, H.; Wang, X.; Chen, P.; Liu, Y.; Zhao, H.; Zhao, Y.; Duan, Y. Low-Temperature Remote Plasma Enhanced Atomic Layer Deposition of ZrO2/Zircone

Nanolaminate Film for Efficient Encapsulation of Flexible Organic Light-Emitting Diodes. *Sci. Rep.* **2017**, *7* (January), 1–9. https://doi.org/10.1038/srep40061.

(41) Piper, D. M.; Travis, J. J.; Young, M.; Son, S. B.; Kim, S. C.; Oh, K. H.; George, S. M.; Ban, C.; Lee, S. H. Reversible High-Capacity Si Nanocomposite Anodes for Lithium-Ion Batteries Enabled by Molecular Layer Deposition. *Adv. Mater.* **2014**, *26* (10), 1596–1601. https://doi.org/10.1002/adma.201304714.

(42) Fischer, A.; Routzahn, A.; George, S. M.; Lill, T. Thermal Atomic Layer Etching: A Review. *J. Vac. Sci. Technol. A* **2021**, *39* (3), 030801. https://doi.org/10.1116/6.0000894.

(43) Benninghoven, A.; Rudenauer, F. G.; Werner, H. W. Secondary Ion Mass Spectrometry–Basic Concepts, Instrumental Aspects, Applications and Trends. *Surf. Interface Anal.* **1987**, *10* (8), 435. https://doi.org/10.1002/sia.740100811.

(44) Van de Heide, P. *Secondary Ion Mass Spectrometry: An Introduction to Principles and Practices*; 2014.

(45) Williams, D. B.; Carter, C. B. The Transmission Electron Microscope. In *Transmission Electron Microscopy*; 1996; pp 3–17. https://doi.org/10.1007/978-1-4757-2519-3_1.

(46) Miller, M. k.; Kenik, E. a. Atom Probe Tomography: A Technique for Nanoscale Characterization. *Microsc. Microanal.* **2004**, *10* (03), 336–341. https://doi.org/10.1017/S1431927604040577.

(47) Priebe, A.; Barnes, J.-P.; Edwards, T. E. J.; Pethö, L.; Balogh, I.; Michler, J. 3D Imaging of Nanoparticles in an Inorganic Matrix Using TOF-SIMS Validated with STEM and EDX. *Anal. Chem.* **2019**, *91*, 11834−11839 Article. https://doi.org/10.1021/acs.analchem.9b02545.

(48) Priebe, A.; Barnes, J.-P.; Edwards, T. E. J.; Huszár, E.; Pethö, L.; Michler, J. Elemental Characterization of Al Nanoparticles Buried under a Cu Thin Film: TOF-SIMS vs STEM/EDX. *Anal. Chem.* **2020**, *92* (18). https://doi.org/10.1021/acs.analchem.0c02361.

(49) Priebe, A.; Sastre, J.; Futscher, M. H.; Jurczyk, J.; Puydinger Dos Santos, M. V.; Romanyuk, Y. E.; Michler, J. Detection of Au+ Ions During Fluorine Gas-Assisted Time-of-Flight Secondary Ion Mass Spectrometry (TOF-SIMS) for the Complete Elemental Characterization of Microbatteries. *ACS Appl. Mater. Interfaces* **2021**. https://doi.org/https://doi.org/10.1021/acsami.1c10352.

(50) van der Heide, P. *X-Ray Photoelectron Spectroscopy: An Introduction to Principles and Practices*; John Wiley & Sons, INC.: Hoboken, NJ, USA, 2012. https://doi.org/10.1002/9781118162897.

(51) Giannuzzi, L. A.; Stevie, F. A. A Review of Focused Ion Beam Milling Techniques for TEM Specimen Preparation. *Micron* **1999**, *30* (3), 197–204. https://doi.org/10.1016/S0968-4328(99)00005-0.

(52) Giannuzzi, L. A.; Stevie, F. A. *Introduction to Focused Ion Beams Instrumentation, Theory, Techniques and Practice*; Springer: New York, 2005.

(53) Mayer, J.; Giannuzzi, L. a; Kamino, T.; Michael, J. TEM Sample Preparation and Damage. *MRS Bull.* **2007**, *32* (5), 400–407. https://doi.org/10.1557/mrs2007.63.

(54) Wang, Z. M. *FIB Nanostructures*; Springer: Heidelberg, 2013.

(55) Dendooven, J.; Detavernier, C. Basics of Atomic Layer Deposition: Growth Characteristics and Conformality. In *Atomic Layer Deposition in Energy Conversion Applications*; John Wiley & Sons, Ltd, 2017; pp 1–40.

https://doi.org/https://doi.org/10.1002/9783527694822.ch1.

(56) Elam, J. W.; Groner, M. D.; George, S. M. Viscous Flow Reactor with Quartz Crystal Microbalance for Thin Film Growth by Atomic Layer Deposition. *Rev. Sci. Instrum.* **2002**, *73* (8), 2981. https://doi.org/10.1063/1.1490410.

(57) Rocklein, M. N.; George, S. M. Temperature-Induced Apparent Mass Changes Observed during Quartz Crystal Microbalance Measurements of Atomic Layer Deposition. *Anal. Chem.* **2003**, *75* (19), 4975–4982. https://doi.org/10.1021/ac030141u.

(58) Langereis, E.; Heil, S. B. S.; Knoops, H. C. M.; Keuning, W.; Van De Sanden, M. C. M.; Kessels, W. M. M. In Situ Spectroscopic Ellipsometry as a Versatile Tool for Studying Atomic Layer Deposition. *J. Phys. D. Appl. Phys.* **2009**, *42* (7). https://doi.org/10.1088/0022-3727/42/7/073001.

(59) Arwin, H.; Aspnes, D. E. Unambiguous Determination of Thickness and Dielectric Function of Thin Films by Spectroscopic Ellipsometry. *Thin Solid Films* **1984**, *113* (2), 101–113. https://doi.org/10.1016/0040-6090(84)90019-1.

(60) Berthomieu, C.; Hienerwadel, R. Fourier Transform Infrared (FTIR) Spectroscopy. *Photosynth. Res.* **2009**, *101* (2–3), 157–170. https://doi.org/10.1007/s11120-009-9439-x.

(61) Smith, B. C. *Fundamentals of Fourier Transform Infrared Spectroscopy*, 1st ed.; CRC Press: Boca Raton, 1995.

(62) Mackus, A. J. M.; Heil, S. B. S.; Langereis, E.; Knoops, H. C. M.; van de Sanden, M. C. M.; Kessels, W. M. M. Optical Emission Spectroscopy as a Tool for Studying, Optimizing, and Monitoring Plasma-Assisted Atomic Layer Deposition Processes. *J.*

Vac. Sci. Technol. A Vacuum, Surfaces, Film. **2010**, *28* (1), 77–87. https://doi.org/10.1116/1.3256227.

(63) Devloo-Casier, K.; Ludwig, K. F.; Detavernier, C.; Dendooven, J. In Situ Synchrotron Based X-Ray Techniques as Monitoring Tools for Atomic Layer Deposition . *J. Vac. Sci. Technol. A Vacuum, Surfaces, Film.* **2014**, *32* (1), 010801. https://doi.org/10.1116/1.4851716.

(64) Werbrouck, A.; Shirazi, M.; Mattelaer, F.; Elliott, S. D.; Dendooven, J.; Detavernier, C. A Secondary Reaction Pathway for the Alumina Atomic Layer Deposition Process with Trimethylaluminum and Water, Revealed by Full-Range, Time-Resolved in Situ Mass Spectrometry. *J. Phys. Chem. C* **2020**, *124* (48), 26443–26454. https://doi.org/10.1021/acs.jpcc.0c07602.

(65) Tai, T. B.; Cao, L.; Mattelaer, F.; Rampelberg, G.; Hashemi, F. S. M.; Dendooven, J.; Van Ommen, J. R.; Detavernier, C.; Reyniers, M. F. Atomic Layer Deposition of Al2O3 Using Aluminum Triisopropoxide (ATIP): A Combined Experimental and Theoretical Study. *J. Phys. Chem. C* **2019**, *123* (1), 485–494. https://doi.org/10.1021/acs.jpcc.8b09198.

(66) Juppo, M.; Rahtu, A.; Ritala, M.; Leskelä, M. In Situ Mass Spectrometry Study on Surface Reactions in Atomic Layer Deposition of TiN and Ti(Al)N Thin Films. *Langmuir* **2000**, *16* (1), 4034-40–39. https://doi.org/https://doi.org/10.1021/la991183+.

(67) Wei, H.; Guo, H.; Sang, L.; Li, X.; Chen, Q. Study on Deposition of Al2O3 Films by Plasma-Assisted Atomic Layer with Different Plasma Sources. *Plasma Sci. Technol.* **2018**, *20* (6). https://doi.org/10.1088/2058-6272/aaacc7.

(68) Kuhs, J.; Hens, Z.; Detavernier, C. Plasma Enhanced Atomic Layer Deposition of

Gallium Sulfide Thin Films. *J. Vac. Sci. Technol. A* **2019**, *37* (2), 020915. https://doi.org/10.1116/1.5079553.

(69) Kuhs, J.; Hens, Z.; Detavernier, C. Plasma Enhanced Atomic Layer Deposition of Aluminum Sulfide Thin Films. *J. Vac. Sci. Technol. A Vacuum, Surfaces, Film.* **2018**, *36* (1), 01A113. https://doi.org/10.1116/1.5003339.

(70) Stevens, E. C.; Mousa, M. B. M.; Parsons, G. N. Thermal Atomic Layer Deposition of Sn Metal Using SnCl 4 and a Vapor Phase Silyl Dihydropyrazine Reducing Agent . *J. Vac. Sci. Technol. A* **2018**, *36* (6), 06A106. https://doi.org/10.1116/1.5055212.

(71) Longrie, D.; Deduytsche, D.; Haemers, J.; Smet, P. F.; Driesen, K.; Detavernier, C. Thermal and Plasma-Enhanced Atomic Layer Deposition of TiN Using TDMAT and NH3 on Particles Agitated in a Rotary Reactor. *ACS Appl. Mater. Interfaces* **2014**, *6* (10), 7316–7324. https://doi.org/10.1021/am5007222.

(72) Scheffe, J. R.; Francés, A.; King, D. M.; Liang, X.; Branch, B. A.; Cavanagh, A. S.; George, S. M.; Weimer, A. W. Atomic Layer Deposition of Iron(III) Oxide on Zirconia Nanoparticles in a Fluidized Bed Reactor Using Ferrocene and Oxygen. *Thin Solid Films* **2009**, *517* (6), 1874–1879. https://doi.org/10.1016/j.tsf.2008.09.086.

(73) King, D. M.; Liang, X.; Zhou, Y.; Carney, C. S.; Hakim, L. F.; Li, P.; Weimer, A. W. Atomic Layer Deposition of TiO2 Films on Particles in a Fluidized Bed Reactor. *Powder Technol.* **2008**, *183* (3), 356–363. https://doi.org/10.1016/j.powtec.2008.01.025.

(74) Poodt, P.; Cameron, D. C.; Dickey, E.; George, S. M.; Kuznetsov, V.; Parsons, G. N.; Roozeboom, F.; Sundaram, G.; Vermeer, A. Spatial Atomic Layer Deposition: A Route towards Further Industrialization of Atomic Layer Deposition. *J. Vac. Sci. Technol. A Vacuum, Surfaces, Film.* **2012**, *30* (1), 010802. https://doi.org/10.1116/1.3670745.

(75) Muñoz-Rojas, D.; Nguyen, V. H.; de la Huerta, C. M.; Aghazadehchors, S.; Jiménez, C.; Bellet, D. Spatial Atomic Layer Deposition (SALD), an Emerging Tool for Energy Materials. Application to New-Generation Photovoltaic Devices and Transparent Conductive Materials. *Comptes Rendus Phys.* **2017**, *18* (7–8), 391–400. https://doi.org/10.1116/1.3670745.

(76) Mackus, A. J. M.; Merkx, M. J. M.; Kessels, W. M. M. From the Bottom-Up: Toward Area-Selective Atomic Layer Deposition with High Selectivity †. *Chem. Mater.* **2019**, *31* (1), 2–12. https://doi.org/10.1021/acs.chemmater.8b03454.

(77) Bobb-Semple, D.; Nardi, K. L.; Draeger, N.; Hausmann, D. M.; Bent, S. F. Area-Selective Atomic Layer Deposition Assisted by Self-Assembled Monolayers: A Comparison of Cu, Co, W, and Ru. *Chem. Mater.* **2019**, *31* (5), 1635–1645. https://doi.org/10.1021/acs.chemmater.8b04926.

(78) Yarbrough, J.; Shearer, A. B.; Bent, S. F. Next Generation Nanopatterning Using Small Molecule Inhibitors for Area-Selective Atomic Layer Deposition. *J. Vac. Sci. Technol. A* **2021**, *39* (2), 021002. https://doi.org/10.1116/6.0000840.

(79) Hu, Y.; Lu, J.; Feng, H. Surface Modification and Functionalization of Powder Materials by Atomic Layer Deposition: A Review. *RSC Adv.* **2021**, *11* (20), 11918–11942. https://doi.org/10.1039/d1ra00326g.

(80) Adhikari, S.; Selvaraj, S.; Kim, D. H. Progress in Powder Coating Technology Using Atomic Layer Deposition. *Adv. Mater. Interfaces* **2018**, *5* (16), 1–20. https://doi.org/10.1002/admi.201800581.

(81) van Ommen, J. R.; Goulas, A. Atomic Layer Deposition on Particulate Materials. *Mater. Today Chem.* **2019**, *14*, 100183. https://doi.org/10.1016/j.mtchem.2019.08.002.

(82) Guerra-Nuñez, C.; Döbeli, M.; Michler, J.; Utke, I. Reaction and Growth Mechanisms in Al2O3 Deposited via Atomic Layer Deposition: Elucidating the Hydrogen Source. *Chem. Mater.* **2017**, *29* (20), 8690–8703. https://doi.org/10.1021/acs.chemmater.7b02759.

(83) Rahtu, A.; Alaranta, T.; Ritala, M. In Situ Quartz Crystal Microbalance and Quadrupole Mass Spectrometry Studies of Atomic Layer Deposition of Aluminum Oxide from Trimethylaluminum and Water. *Langmuir* **2001**, *17* (21), 6506–6509. https://doi.org/10.1021/la010103a.

(84) Heil, S. B. S.; Kudlacek, P.; Langereis, E.; Engeln, R.; Van De Sanden, M. C. M.; Kessels, W. M. M. In Situ Reaction Mechanism Studies of Plasma-Assisted Atomic Layer Deposition of Al2O3. *Appl. Phys. Lett.* **2006**, *89*, 131505-1-131505–3. https://doi.org/10.1063/1.2357886.

(85) Shirazi, M.; Elliott, S. D. Cooperation between Adsorbates Accounts for the Activation of Atomic Layer Deposition Reactions. *Nanoscale* **2015**, *7* (14), 6311–6318. https://doi.org/10.1039/c5nr00900f.

(86) Klejna, S.; Elliott, S. D. First-Principles Modeling of the “Clean-up” of Native Oxides during Atomic Layer Deposition onto III-V Substrates. *J. Phys. Chem. C* **2012**, *116* (1), 643–654. https://doi.org/10.1021/jp206566y.

(87) Elliott, S. D.; Greer, J. C. Simulating the Atomic Layer Deposition of Alumina from First Principles. *J. Mater. Chem.* **2004**, *14* (21), 3246–3250. https://doi.org/10.1039/b405776g.

(88) Pasynkiewicz, S.; Boleslawski, M. Synthesis of Trimethylaluminium. *J. Organomet. Chem.* **1970**, *25* (1), 29–32. https://doi.org/10.1016/S0022-328X(00)86201-4.

(89) Priebe, A.; Pethö, L.; Michler, J. Fluorine Gas Coinjection as a Solution for Enhancing Spatial Resolution of Time-of-Flight Secondary Ion Mass Spectrometry and Separating Mass Interference. *Anal. Chem.* **2020**, *92*, 2121–2129. https://doi.org/https://doi.org/10.1021/acs.analchem.9b04647.

For Table of Contents Only